ADVANCED ELECTRONIC MATERIALS

Supporting Information

for *Adv. Electron. Mater.*, DOI: 10.1002/aelm.201600473

Size Dependence of Electrical Conductivity and Thermoelectric Enhancements in Spin-Coated PEDOT:PSS Single and Multiple Layers

*Virgil Andrei, Kevin Bethke, Fani Madzharova, Sebastian Beeg, Axel Knop-Gericke, Janina Kneipp, and Klaus Rademann**

Supporting information for: Size dependence of electrical conductivity and thermoelectric enhancements in spin-coated PEDOT:PSS single and multiple layers

Virgil Andrei,[†,§] Kevin Bethke,[†] Fani Madzharova,[†] Sebastian Beeg,[‡,¶] Axel Knop-Gericke,[‡] Janina Kneipp,[†] and Klaus Rademann[*,†]

Department of Chemistry, Humboldt-Universität zu Berlin, Brook-Taylor-Straße 2, 12489 Berlin, Germany., Department of Inorganic Chemistry, Fritz-Haber-Institut der Max-Planck-Gesellschaft, Faradayweg 4–6, 14195 Berlin, Germany., and Department of Heterogeneous Reactions, Max-Planck-Institute for Chemical Energy Conversion, Stiftstraße 34-36, 45470 Mülheim an der Ruhr, Germany.

E-mail: klaus.rademann@chemie.hu-berlin.de

Phone: +49 30/2093-5565. Fax: +49 30/2093-5559

[*]To whom correspondence should be addressed

[†]Department of Chemistry, Humboldt-Universität zu Berlin, Brook-Taylor-Straße 2, 12489 Berlin, Germany.

[‡]Department of Inorganic Chemistry, Fritz-Haber-Institut der Max-Planck-Gesellschaft, Faradayweg 4–6, 14195 Berlin, Germany.

[¶]Department of Heterogeneous Reactions, Max-Planck-Institute for Chemical Energy Conversion, Stiftstraße 34-36, 45470 Mülheim an der Ruhr, Germany.

[§]Current address: Department of Chemistry, University of Cambridge, Lensfield Road, Cambridge CB2 1EW, UK.

Contents

1 Additional sample preparation details

The details of the employed chemicals are given in Table S1. The square glass plates (1 mm thick, with 25 mm long edges) are obtained from microscope slides (ROTH), using a Diamond glass cutter.

Table S1: Specifications of the used chemicals, as given on the vendors' websites.

Substance	Other names	Vendor	Specifications
PEDOT:PSS	Orgacon^{TM} DRY	Sigma-Aldrich (Agfa-Gevaert)	dry re-dispersible pellets 200-450 Ω/sq mp >300 °C Virtually 100% absorption from 900-2000 nm. No absorption maximum from 400-800 nm. Visual Light Transmission: ∼85%.
DMSO	Dimethyl sulfoxide ROTIPURAN®	ROTH	≥99.8 %, p.a. M 78.13 g/mol; ρ ∼1.1 g/mL Flp 87 °C; Kp ≈189 °C

For the spin-coating, two drops of the polymeric solutions are first spread over the top glass surface using the tip of a smooth glass rod.

An example for a PP5D sample is shown in Fig. S1, where the two silver stripes and three black markings are visible. The markings are made on the backside of the supporting glass, to indicate the position of the film scratches for the AFM measurements (Section 4).

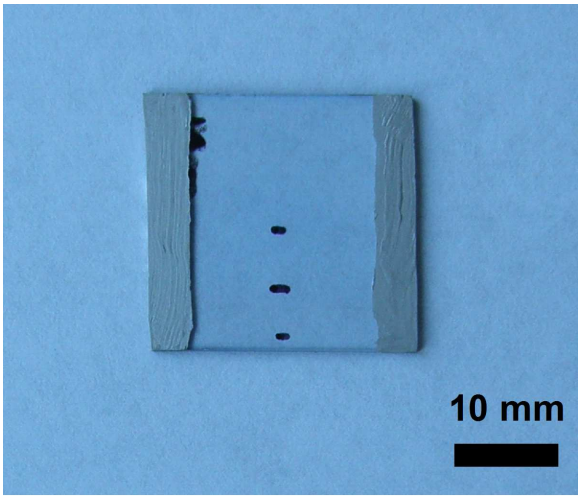

Figure S1: Picture of a thin PEDOT:PSS film on glass.

2 Seebeck coefficient measurements

Two Peltier elements are employed to set a temperature difference between the two ends of the sample. At the upper side of both elements, two temperature sensors record the achieved temperature, which allows a proportional–integral–derivative (PID) controller to regulate the delivered power. In this way, a fast thermal equilibrium is obtained. At the lower end, two aluminum heat dissipators ensure that the excess heat is being removed. The voltage values are registered by a Fluke 289 multimeter, which transfers the raw data to a computer through an infrared-USB adapter cable. A custom made program is employed to control the measurement sequence and record the data points, which are saved once every second.

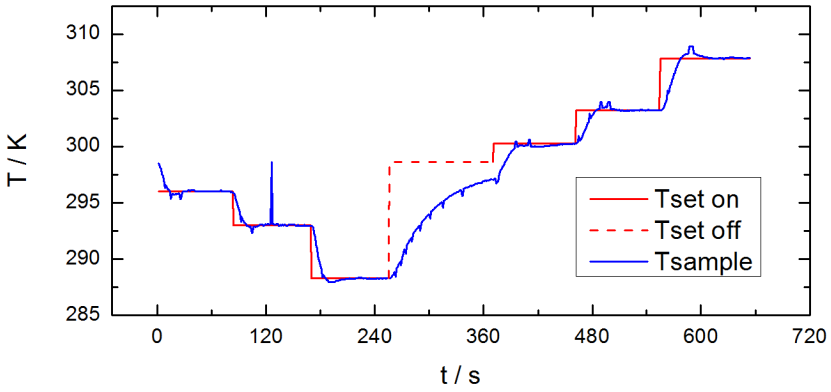

Figure S2: The step-wise changes of the temperature during a single measurement cycle (three cycles are recorded for calculating the Seebeck coefficient). The red line indicates the desired temperature (Tset), while the blue line represents the temperature achieved by the heating plates without a sample (in air), as registered by the attached thermometers (Tsample).

The measurement sequence consists of three temperature steps for both heating and cooling, as shown in Fig. S2. To ensure a thermal equilibrium at each step, the PID controller maintains a constant temperature for 60 s, after first stabilizing it. Since other electrochemical or capacitive processes can also induce an electrical potential, this sequence reveals whether the Seebeck effect is the only cause for the signal. If this is the case, the recorded voltage also changes its sign during the measurement, mirroring the aspect of the temperature

curve. The intermediate step between the heating and the cooling runs allows the sample to return at room temperature. This period is required for a smooth transition between different temperatures, which eliminates effects such as hysteresis. This sequence is recorded three times for each thin sample, to have a statistical evidence over the reproducibility of the measurements.

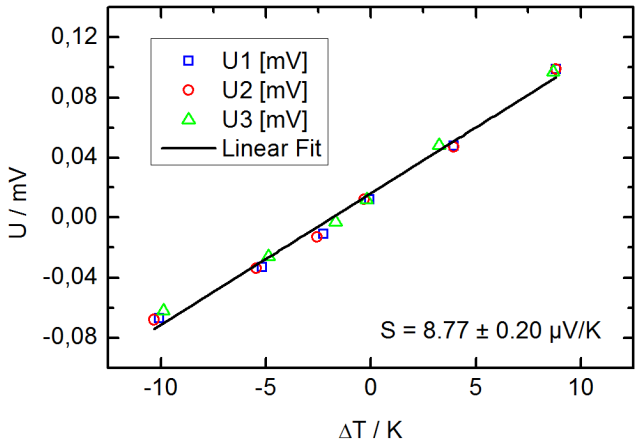

Figure S3: Determination of the room temperature Seebeck coefficient by linear regression for a PP5D sample.

Since the thermoelectric voltage is linearly dependent on the temperature difference in a small interval of 5-20 K, the room temperature Seebeck coefficient is calculated through the differential method for all samples.[S1] An example is shown in Fig. S3, which presents the three recorded series of points for a single PP5D thin film (v2 = 2000 RPM).

3 Determination of the electrical resistance

The electrical resistance is determined in a quasi-4-point configuration, using the setup illustrated in Fig. S4a. The sample is held on top of a measurement block by a 625 g weight. The 48 g block consists of four parallel copper wires, which are embedded in a plastic holder and polished at the same height (see Fig. S4b). The two pairs of electrodes of the VersaSTAT3 current source are connected to the two outer copper wires, serving as both current source and voltage sensors. The VersaSTAT3 instrument is controlled through the software VersaStudio 2.44.4, using a programmable measurement sequence. In this case, a chronopotentiometric sequence is employed, which maintains a constant current, while registering the voltage values once every second, for 30 s.

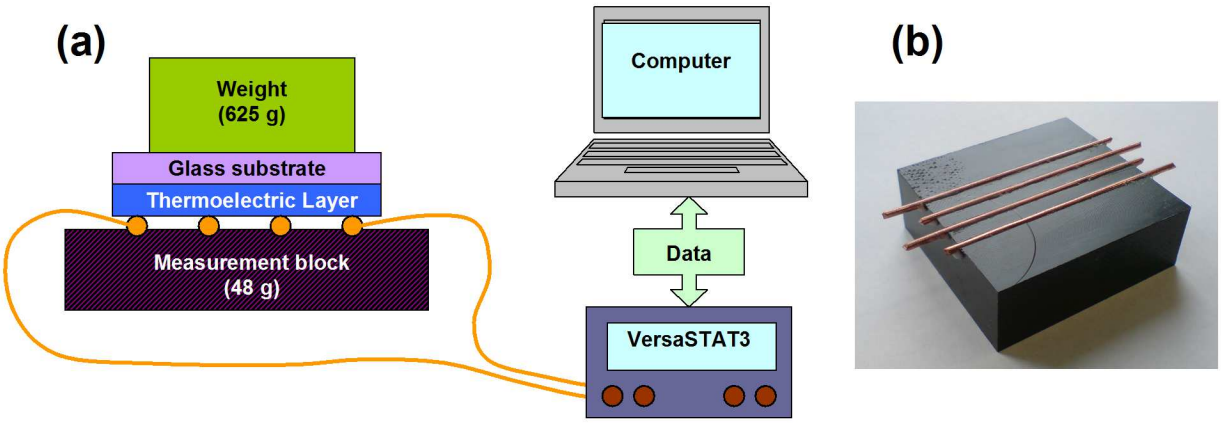

Figure S4: (a) Setup employed to determine the electrical conductivity of thin samples. The measurements are conducted using the quasi-4-point method. (b) Photographic image of the measurement block, which is used throughout the thermoelectric investigations of thin samples.

An example of the obtained results is illustrated in Fig. S5, which shows the points recorded at room temperature for a pristine PEDOT:PSS thin layer. In order to calculate the electrical conductivity, these data points are statistically handled, as described in Section 8.

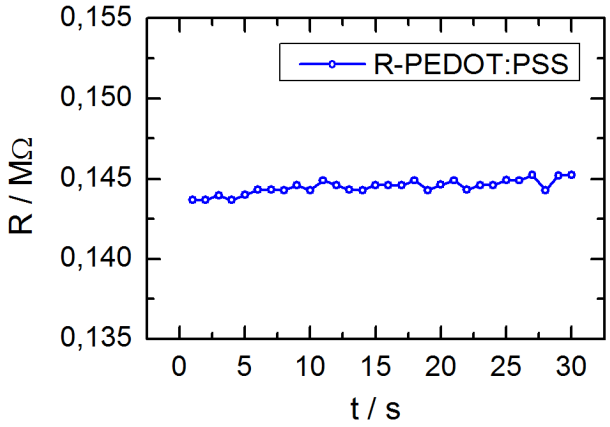

Figure S5: Raw electrical resistance data for a PEDOT:PSS thin film, at room temperature.

4 Atomic force microscopy

The determination of the electrical conductivity also requires knowing the thickness (h) of the thin samples. For this purpose, atomic force microscopy (AFM) is implemented. This versatile method presents several advantages over other techniques (e.g. profilometry), such as the acquisition of three dimensional information and its tunability regarding the spacial resolution and scan speed, resulting in a higher precision.

For the determination of the sample thickness, the films are first scratched using a common sewing needle, at approximately 1 mm, 6 mm and 12 mm from the edge of the sample. In this way, the result takes into account the radial distribution of the thickness, along the rotation axis of the glass plate. The position of these three points is visible from Fig. S1, where they are marked black. A typical example of such a scratch can be also observed in Fig. S6, where the output from the software Gwyddion is revealed for a diethylene glycol (DEG) treated PEDOT:PSS sample. The scratches result in well defined depth profiles, where the polymer layers can be well distinguished from the underlying glass substrate. The two central traces correspond to the scratches in glass, which are left by the needle tip. Among the sections, where clear profiles can be determined (see the white line), several polymer folds are also visible. Such folds represent leftovers from the shearing force of the needle on the soft polymer layer. Since those folds are often responsible for the so-called

horizontal scars (or strokes), a slow scan speed is required, in order to obtain a good visual representation of the surface. For this high-resolution example, a scan speed of 1/6 lines per second is chosen, with 512 points recorded per line.

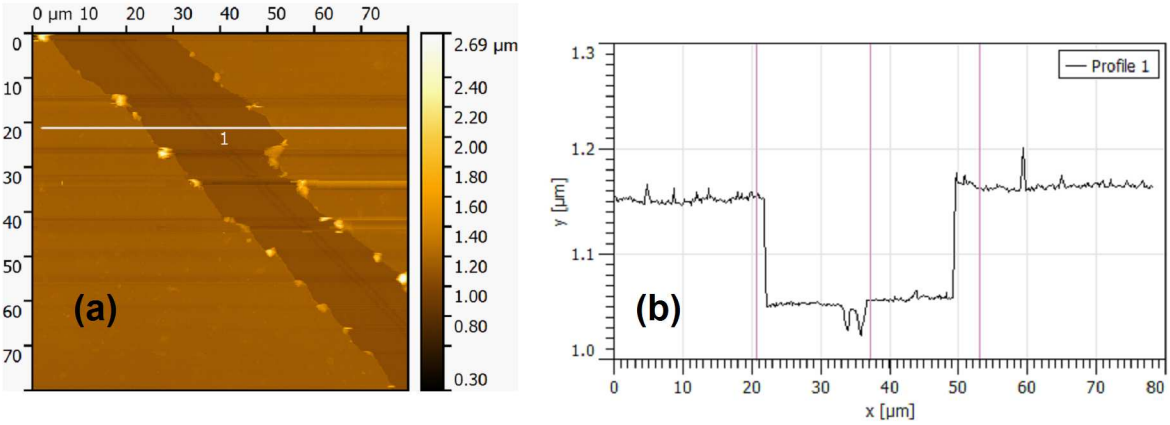

Figure S6: Typical output from the software Gwyddion. (a) The AFM image reveals various common features of all samples, such as the depth profile of the thin films, deeper glass scratches, polymer folds and the resulting horizontal scars. (b) The two dimensional depth profile corresponds to the white line in frame (a).

Although the above mentioned parameters are more favorable for obtaining few horizontal scars, they result in an increased measuring time. Since only a single depth profile is required for one scratch, a comparison is made between the various profiles of a pristine PEDOT:PSS sample. In this case, the surfaces are scanned at a constant rate of 1 line per second, with either 512 or 128 points per line. The results can be seen in Fig. S7, where the designations *inner* (S7a), *middle* (S7b) and *outer* (S7c) refer to the relative positions of the scratches from the edge of the glass plate, at 12 mm, 6 mm and 1 mm, respectively. Due to the higher scan speed, a non-symmetric curving of the planar surface is sometimes observed (e.g. S7a). In order to compensate for the resulting asymmetry, the film depth is recorded as the average of the two thickness values, from each side of the scratch. Nevertheless, these deviations are within the error caused by the radial distribution, as shown in Fig. S7d. Since there is no significant difference between the results for the two spacial resolutions (128×128, respectively 512×512 points), the faster 128×128 images are chosen for all further

investigations.

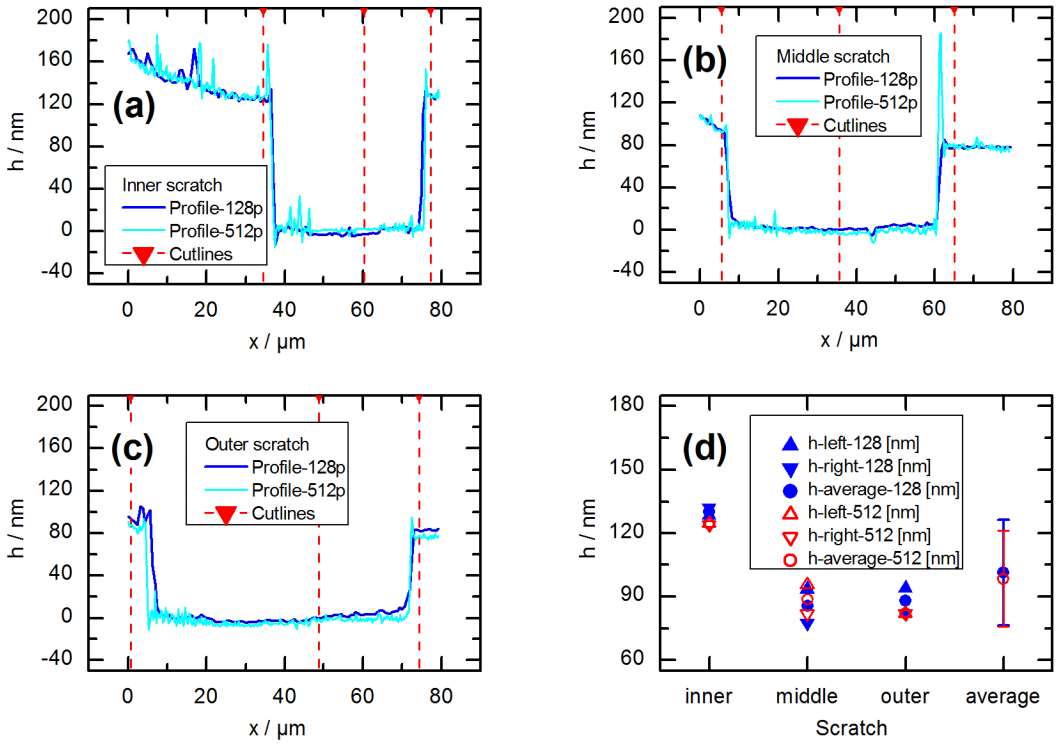

Figure S7: (a-c) Comparison between the depth profiles of a PEDOT:PSS sample, recorded at different parameters. (d) Comparison between the individual data points delivered at the two spacial resolutions (128×128 and 512×512 pixels). The uncertainty caused by the radial distribution of the polymer is significantly higher than the asymmetry between the left and right edges of a depth profile.

5 Ultraviolet-visible light spectroscopy

The recorded UV-Vis spectra are given in Fig. S8. The absorbance is gradually increasing for a lower spin-coating speed (see frame S8a for the PP layers, and S8c for the PP5D ones). An even larger difference is noticeable for the multiple layers (S8b, respectively S8d), where the absorbance depends almost linearly on the number of layers, with deviations caused by the radial distribution in the film thickness.

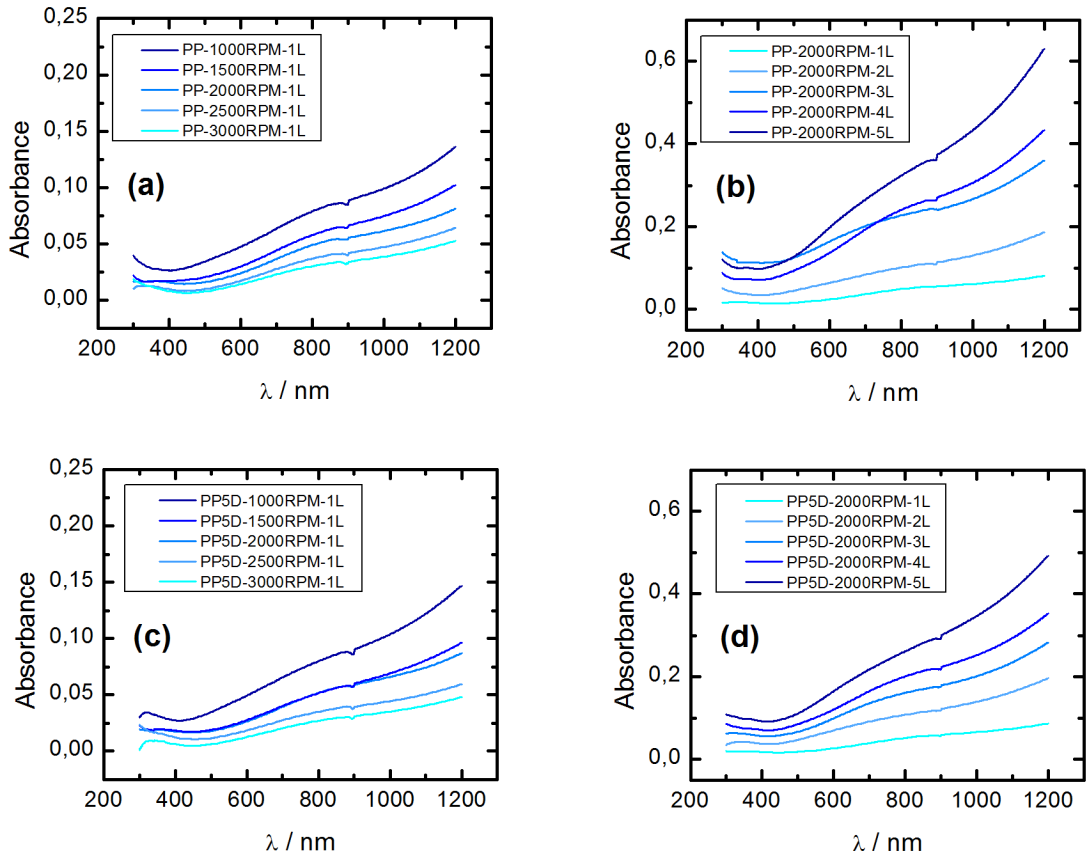

Figure S8: UV-Vis spectra of the various PEDOT:PSS thin films. (a) PP solution, at different spin-coating speeds; (b) multiple layered films obtained using a PP solution; (c) PP5D solution, at different spin-coating speeds; (d) multiple layered films from a PP5D solution. Darker blue tones of the UV-Vis spectra indicate thicker films.

The UV-Vis absorption bands of PEDOT:PSS are also assigned in Table S2, according to literature. Further irregularities at around 300 nm are caused by the absorbance of the glass substrates, while those at approximately 900 nm are caused by the Jasco V-670

UV-Vis Spectrophotometer instrument. Otherwise, the minimal absorbance in the shorter wavelength interval of 300-600 nm is responsible for the dark blue color of PEDOT:PSS.

Table S2: UV-Vis absorption bands of PEDOT:PSS thin films, as described in the literature.

Band	λ / nm
$PEDOT^{2+}$ bipolaron[S2,S3]	broad NIR absorption band
$PEDOT^{+}$ polaron[S2,S3]	900
$PEDOT^{0}$ neutral[S2,S3]	600

6 Raman spectroscopy

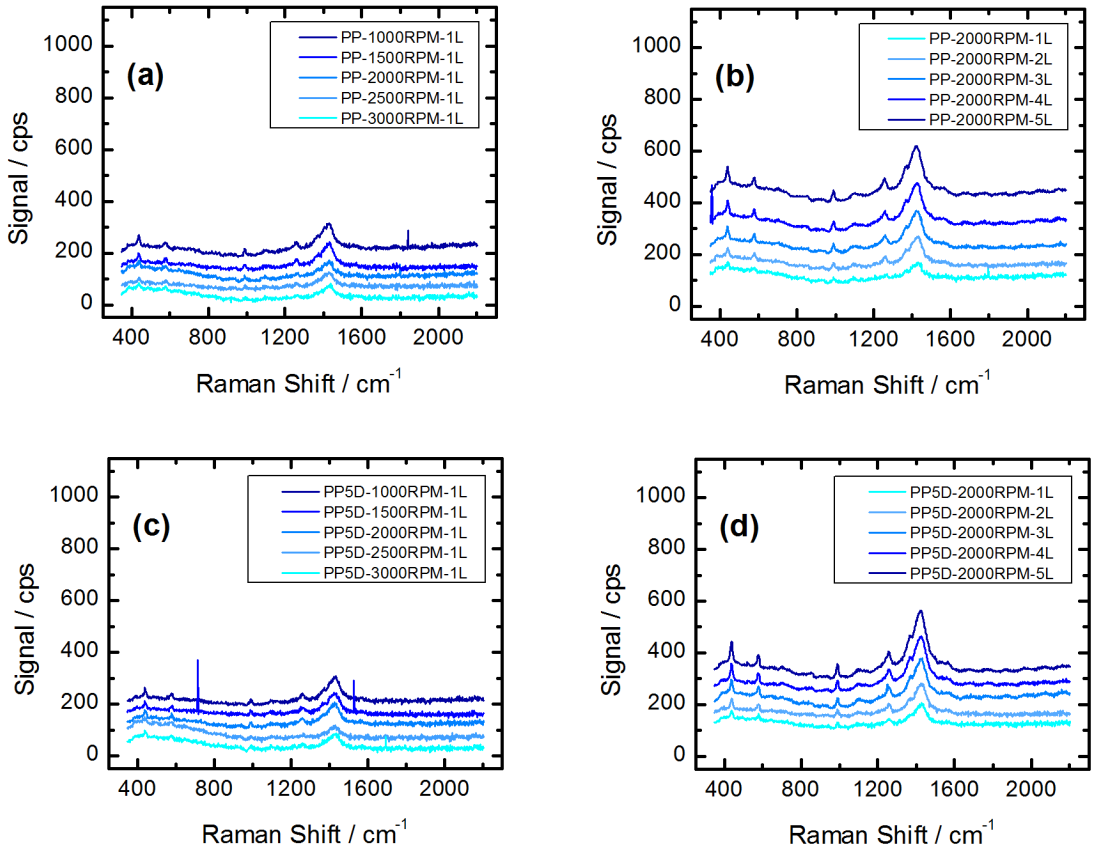

Figure S9: Raman spectra for the investigated PEDOT:PSS layers. (a) PP solution, at different spin-coating speeds; (b) multiple layered films obtained using a PP solution; (c) PP5D solution, at different spin-coating speeds; (d) multiple layered films from a PP5D solution. The Raman spectra are shifted vertically by an arbitrary value, in order to avoid overlapping and to improve visibility. Darker blue tones of the Raman spectra indicate thicker films.

In order to obtain the exact position of the Raman bands, a 4 point fast Fourier transform (FFT) filter is employed. The Origin function smooths the recorded signal, removing the signal noise. Consequently, the function "Peak Analyzer" is used to identify the maximal values of the smoothed curves. Examples are found in Fig. 7b from the main article for the PP films and in Fig. S10 for the PP5D samples.

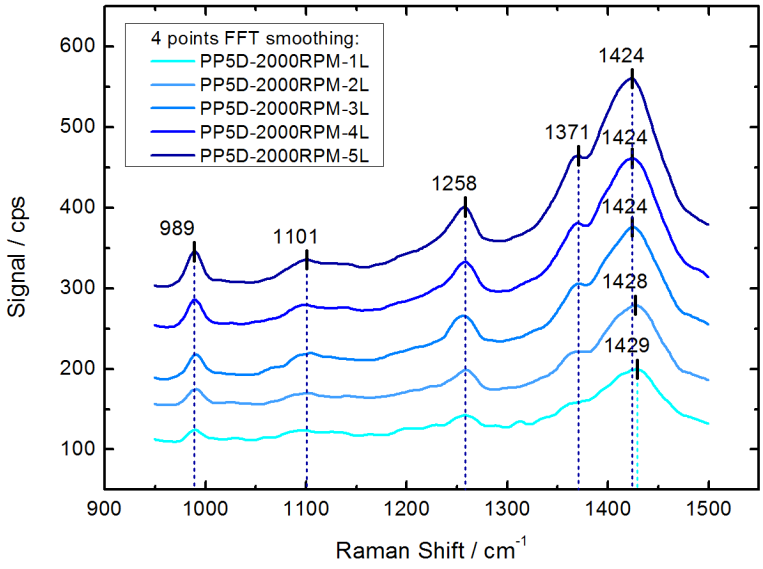

Figure S10: The maxima in the main Raman bands of the multi-layered PP5D films, as determined after smoothing the signal noise with a 4 point FFT filter. The Raman spectra are shifted vertically by an arbitrary value, in order to avoid overlapping and to improve visibility. Darker blue tones of the Raman spectra indicate thicker films.

7 X-ray photoelectron spectroscopy

The XPS spectra are recorded as described in the main article. The S(2p) core level spectra of the PP5D sample set is displayed in Fig. S11, giving an overview of the sulfur S(2p) photoelectric line behavior. The position of the p doublet peaks (p1/2 and p3/2) of two different sulfur species can be obtained from their fit, as exemplified in Fig. S12 for a five-layered PP sample. For a more detailed overview, both sample sets are compared according to the number of spin-coating procedures in Fig. S13. No clear changes in the relative peak heights were detected.

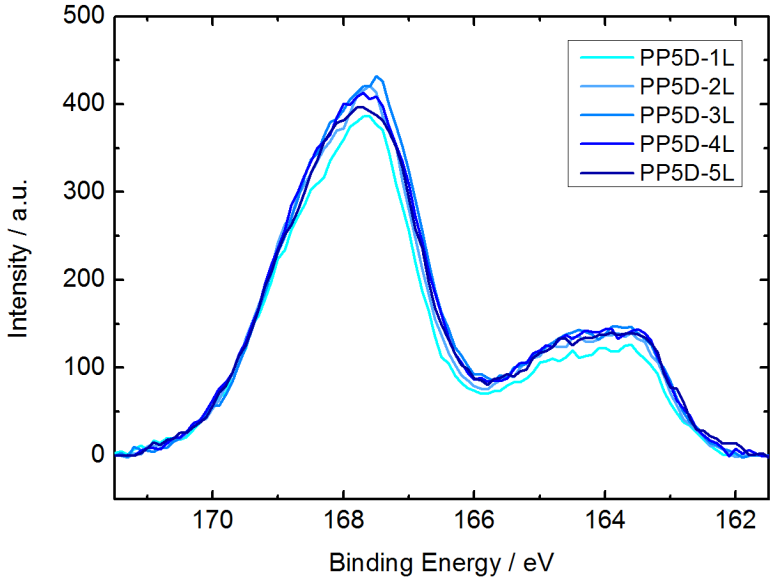

Figure S11: S(2p) core level XPS spectra of the PP5D sample set after Shirley background subtraction.

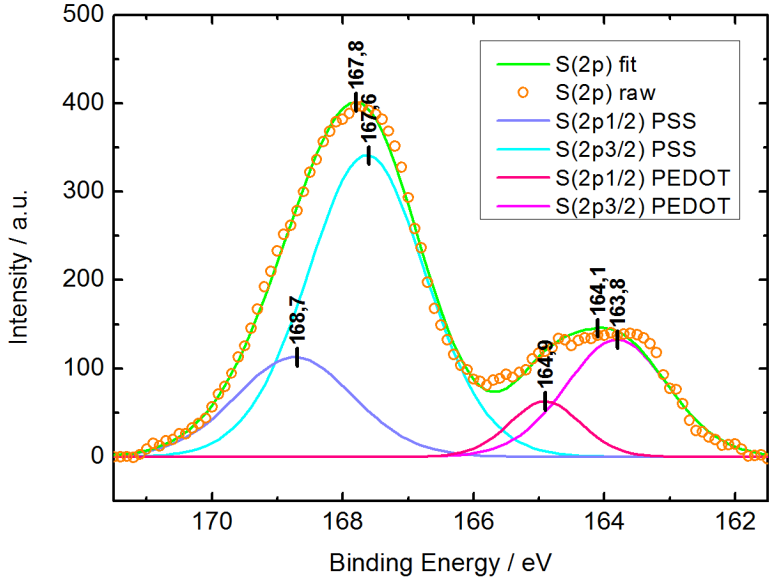

Figure S12: Fitting and deconvolution of the S(2p) core level XPS spectra for a five-layered PP sample.

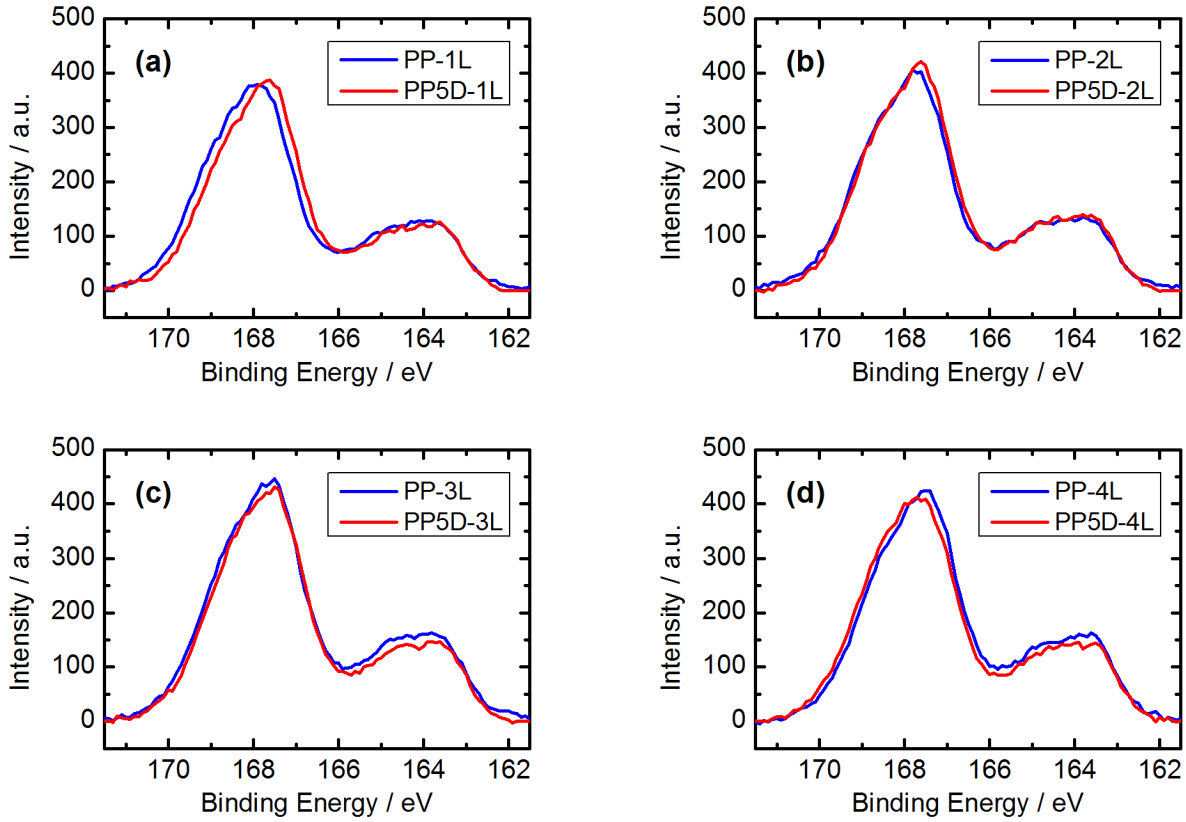

Figure S13: Comparison between the S(2p) core level XPS spectra of the PP and PP5D samples with the same number of layers. The spectra of the five-layered films are plotted in Fig. 8b from the main article.

The composition of the surface-near region is shown in Tables S3 and S4. The different elemental contents are displayed in percentages and vary approx. by ±1%. In both sample sets (PP, PP5D) the first two samples exhibit small amounts of silicon, probably originating from the substrate. Since in both sample sets, this amount decreases for the second sample, it is possible that the whole surface is not homogeneously covered under a thick PEDOT:PSS layer of around 100 nm (see Fig. 3b from the main article). The slightly increased oxygen content for the first samples of both sample sets is also presumably related to the silicon substrate. Additionally for the first two samples of the PP sample set, a slight shift towards higher binding energy (BE) is visible. This might be related to a thin PEDOT:PSS over layer interacting with the underlying silicon substrate. Except for the very first sample of both sample sets, all samples show small amounts of fluorine present on the surface. Residual amounts of sodium and chlorine are also detected.

Table S3: Surface-near molar ratios and atomic percentages of the PP samples according to XPS.

Sample	PP-1L	PP-2L	PP-3L	PP-4L	PP-5L
Ratio S_{PEDOT}:S_{PSS}	0.35	0.34	0.36	0.36	0.37
Atom [%]					
O	24	23	23	22	22
S_{PSS}	6	7	7	7	7
S_{PEDOT}	2	2	2	2	2
Na	3	2	2	2	2
F	0	2	2	2	2
C	59	60	61	62	62
Cl	0	1	0	0	0
N	2	2	3	3	3
Si	4	1	0	0	0
Total	100	100	100	100	100

The analysis of the sulfur photoelectronic peak allows the identification of thiophene sulfur at lower binding energy (S_{PEDOT}) and the sulfur species originating from the sulfonated PSS polymer chains at higher binding energy (S_{PSS}).[S4] For a greater S_{PEDOT}:S_{PSS} ratio number, a lower PSS content can be assumed at the sample surface. The ratios are displayed

Table S4: Surface-near molar ratios and atomic percentages of the PP5D samples according to XPS.

Sample	PP5D-1L	PP5D-2L	PP5D-3L	PP5D-4L	PP5D-5L
Ratio S_{PEDOT}:S_{PSS}	0.32	0.33	0.32	0.33	0.34
Atom [%]					
O	24	22	22	22	23
S_{PSS}	6	6	6	6	6
S_{PEDOT}	2	2	2	2	2
Na	3	2	2	2	1
F	0	2	2	2	2
C	61	62	62	63	63
Cl	0	0	1	0	0
N	2	3	3	3	3
Si	2	1	0	0	0
Total	100	100	100	100	100

in Tables S3 and S4, above the surface elemental composition data. The ratios vary only slightly for both PP and PP5D samples, indicating that no significant change occurs at the near-surface region. Still, the accuracy range of the composition analysis prevents a further interpretation of the acquired data.

8 Statistic data interpretation

The average value ($\bar{S}$) and the uncertainty (e_S) of the Seebeck coefficient are determined from the linear regression through the measured data points. These two results are taken from Origin, without further handling. The average electrical resistance ($\bar{R}$) and its uncertainty (e_R) at room temperature are calculated with the help of Eq. (1) and Eq. (2), with $n = 30$.[S5] The average height ($\bar{h}$) and the corresponding uncertainty (e_h) of nanometer thin layers are also determined in this way, with $n = 3$. The acquisition of three individual points from the depth profiles of each sample is explained in detail in Section 4.

$$\bar{R} = \frac{\sum_{i=1}^{n} R_i}{n} \tag{1}$$

$$e_R = \sqrt{\frac{\sum_{i=1}^{n} (R_i - \bar{R})^2}{n-1}} \tag{2}$$

Having this information, the average value ($\bar{\sigma}_{thin}$) of the electrical conductivity can be calculated with the help of Eq. (3) for the thin layers. The width of the samples corresponds to that of the supporting glass ($w = 25\,\mathrm{mm}$), while the length between the two conductive stripes is also constant ($l = 17\,\mathrm{mm}$). Eq. (4) is further employed for the calculation of the uncertainty in σ_{thin}.

$$\bar{\sigma}_{thin} = \frac{l}{w \cdot \bar{h} \cdot \bar{R}} \tag{3}$$

$$\%e_{\sigma_{thin}} = \sqrt{\%e_h^2 + \%e_R^2} \tag{4}$$

For the calculation of the uncertainty in the power factor ($\bar{PF} = \bar{\sigma}\bar{S}^2$), Eq. (5) is employed. Eq. (4) and (5) are mathematically derived from the general case, which is shown in

Eq. (6). F is a function of the experimental variables x, y, z, ...[S6]

$$\%e_{PF} = \sqrt{\%e_{\sigma}^2 + \%e_S^2 \cdot 4} \tag{5}$$

$$e_{F(x,y,z,...)} = \sqrt{\left(\frac{\partial F}{\partial x}\right)^2 \cdot e_x^2 + \left(\frac{\partial F}{\partial y}\right)^2 \cdot e_y^2 + \left(\frac{\partial F}{\partial z}\right)^2 \cdot e_z^2 + ...} \tag{6}$$

9 Comparison with common σ enhancement strategies

The treatment with polar solvents is an established method for obtaining very high conductivities, resulting in the reorganization and washing of the upper surface. Although an improvement should be also observed when only using the solvents, some significant differences must be emphasized between this case and our experiments. For pure solvents, the reorganization of PEDOT is mainly driven by the solvation and removal of the excess PSS chains from the surface, where the latter results in a decreased film thickness and accordingly in an even higher electrical conductivity. This PSS removal is particularly favored by the difference in concentration and pH (pH≈1-2 for PSS), which does not occur when using a typically concentrated PEDOT:PSS solution. In literature, the mass loss is best observed from the changing S_{PEDOT}:S_{PSS} ratio number of the respective XPS peaks. As already mentioned in the main article, no such change is visible in the XPS spectra, which indicates that the chain reorganization is the deciding factor, rather than the PSS removal. This is also supported by the AFM measurements, which show an almost linear increase in thickness, without mass losses. When only using solvent instead of a PEDOT:PSS solution, the gradual mass loss (caused by the repeated washing) would be the main modification to the films, resulting in very different layers to ours.

Still, the results are also compared to other common strategies for enhancing the electrical conductivity, in order to demonstrate that the reported improvements are not only based on the reorganization and washing of the polymer chains. As a control experiment, the proven

approach of treating a pristine PEDOT:PSS layer with DMSO (noted PP-1L-DMSO) is employed, which can remove PSS far better than water containing 5 vol.% DMSO. As it can be seen in Fig. S14, the thickness of a DMSO treated sample is decreased by around 20%, while its electrical conductivity (175 cm^{-1}) surpasses that of the corresponding PP5D single layer. Nevertheless, the conductivities of the PP5D multiple layers (≈200 cm^{-1}) are superior to that of the DMSO treated layer, indicating that the reorganization is not the only effect contributing to the enhancement. This becomes even more obvious when comparing the PP5D samples with a DMSO treated sample which has been dried in oven for one hour, instead of 5 minutes (PP-1L-DMSO-1h). In that case, almost no enhancement is observed in comparison to a PP5D single layer.

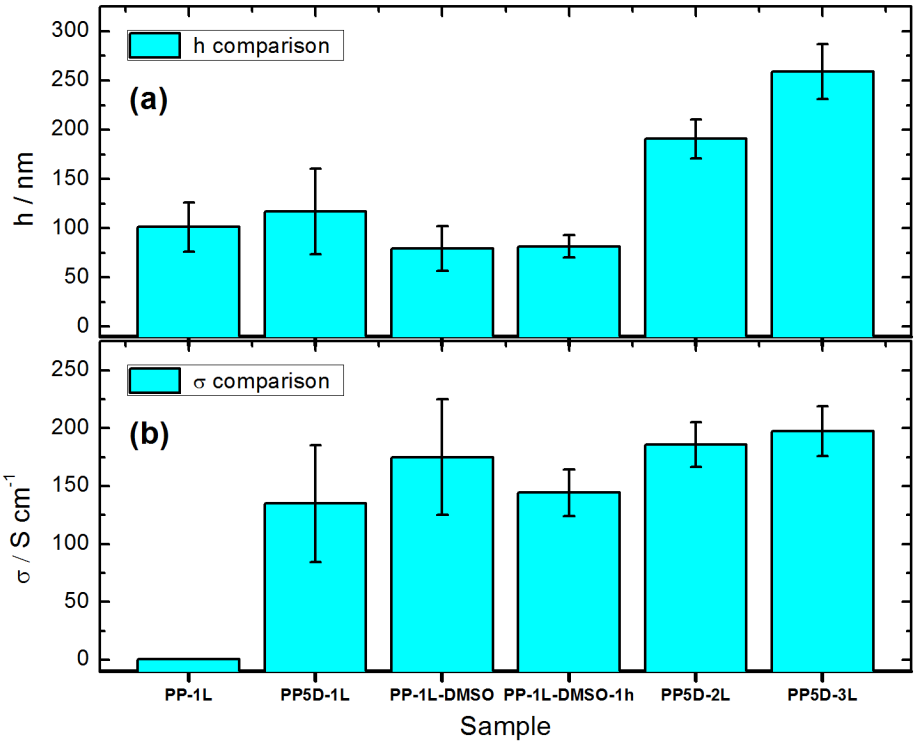

Figure S14: Comparison between various types of samples: (a) film thickness, (b) electrical conductivity. While the DMSO surface treatment decreases the film thickness of the respective samples (PP-1L-DMSO, PP-1L-DMSO-1h), the resulting conductivities do not surpass the values of the PP5D multiple layers.

References

(S1) Martin, J.; Tritt, T.; Uher, C. *J. Appl. Phys.* **2010**, *108*.

(S2) Luo, J.; Billep, D.; Waechtler, T.; Otto, T.; Toader, M.; Gordan, O.; Sheremet, E.; Martin, J.; Hietschold, M.; Zahn, Dietrich R. T.,; Gessner, T. *J. Mater. Chem. A* **2013**, *1*, 7576–7583.

(S3) Liu, S.; Deng, H.; Zhao, Y.; Ren, S.; Fu, Q. *RSC Adv.* **2015**, *5*, 1910–1917.

(S4) Mengistie, D. A.; Chen, C.-H.; Boopathi, K. M.; Pranoto, F. W.; Li, L.-J.; Chu, C.-W. *ACS Appl. Mater. Interfaces* **2015**, *7*, 94–100.

(S5) Andrei, V.; Bethke, K.; Rademann, K. *Phys. Chem. Chem. Phys.* **2016**, *18*, 10700–10707.

(S6) Harris, D. C. *Quantitative chemical analysis*, 7th ed.; W.H. Freeman and Co.: New York and NY, 2007.